Applied Physics Letters

Line-length-dependent dislocation glide in refractory multi-principal element alloys

Cite as: Appl. Phys. Lett. **120**, 061901 (2022); https://doi.org/10.1063/5.0080849
Submitted: 03 December 2021 • Accepted: 24 January 2022 • Published Online: 07 February 2022

Shuozhi Xu, Wu-Rong Jian, Yanqing Su, et al.

COLLECTIONS

Note: This paper is part of the APL Special Collection on Metastable High Entropy Alloys.

This paper was selected as an Editor's Pick

Applied Physics Letters ARTICLE scitation.org/journal/apl

Line-length-dependent dislocation glide in refractory multi-principal element alloys

Cite as: Appl. Phys. Lett. **120**, 061901 (2022); doi: 10.1063/5.0080849
Submitted: 3 December 2021 · Accepted: 24 January 2022 ·
Published Online: 7 February 2022

Shuozhi Xu,[1,a] Wu-Rong Jian,[1] Yanqing Su,[2] and Irene J. Beyerlein[1,3]

AFFILIATIONS

[1]Department of Mechanical Engineering, University of California, Santa Barbara, California 93106-5070, USA
[2]Department of Mechanical and Aerospace Engineering, Utah State University, Logan, Utah 84322-4130, USA
[3]Materials Department, University of California, Santa Barbara, California 93106-5050, USA

Note: This paper is part of the APL Special Collection on Metastable High Entropy Alloys.
[a]**Author to whom correspondence should be addressed:** shuozhixu@ucsb.edu

ABSTRACT

Plastic deformation of refractory multi-principal element alloys (RMPEAs) is known to differ greatly from those of refractory pure metals. The fundamental cause is the different dislocation dynamics in the two types of metals. In this Letter, we use atomistic simulations to quantify dislocation glide in two RMPEAs: MoNbTi and NbTiZr. Edge and screw dislocations on the {110} and {112} slip planes are studied. A series of dislocation line lengths, ranging from 1 nm to 50 nm, are employed to elucidate the line-length-dependence. To serve as references, the same simulations are performed on pure metals. For the RMPEAs, the dependence of critical stresses on length becomes undetectable within the statistical dispersion for dislocations longer than 25 nm, as a result of the change in dislocation behavior. This length is in good agreement with those predicted by analytical models. Compared to the pure metals, the critical stress anisotropy among different slip planes and character angles is substantially reduced, providing an explanation for the homogeneous plasticity in RMPEAs observed in prior experiments.

Dislocation gliding in body-centered cubic (BCC) pure metals has been studied extensively. At low temperatures, a long screw dislocation (> 1 nm) is known to glide via the kink-pair mechanism.[1] Kink-pair migration was also found during long edge dislocation gliding in BCC Fe[2–5] and Mo,[6] yet with less pronounced kinks. For example, on the {110} plane in Fe, the kink width on an edge dislocation, 0.7 or 1.5 nm,[2,3] is smaller than that on a screw dislocation, 4, 4.8, 5, or 6 nm.[3,7–10] For edge dislocations in Fe, the kinks on {112} planes are more pronounced than those on {110} planes.[4,5] Since a longer dislocation (tens of nm) can contain more kinks, its critical resolved shear stress (CRSS) is usually lower than that of a short one (≈1 nm) of the same character.[11] For the same length, the CRSS of a screw dislocation is at least one order of magnitude higher than that of its edge counterpart.[12] A practical result of all these dislocation behaviors is that plasticity in BCC pure metals at low temperatures is mainly controlled by the gliding of screw dislocations.

The motion of long dislocations in BCC refractory multi-principal element alloys (RMPEAs)[13] is more complicated. First, subject to zero applied stress, the static screw dislocation core in RMPEAs can be compact or non-compact, depending on the local chemical environment.[14–16] This contrasts the compact static core structure of the screw dislocation in multiple BCC pure metals.[17,18] As a result of the chemistry-dependent core structure, partial kinks are spread on varying {110} planes along the screw dislocation line. Consequently, screw dislocation glide in RMPEA is controlled by cross kinks, i.e., collision of kinks on different glide planes,[19,20] instead of kink-pair formation as in BCC pure metals. Wavy screw dislocations in RMPEAs have been confirmed by transmission electron microscopy (TEM) experiments.[21] Edge dislocation glide in RMPEAs is also significantly affected by kinks,[22] which are much more pronounced than those in BCC pure metals. Therefore, the screw-to-edge ratio in CRSS is significantly lowered in RMPEAs and BCC concentrated binary alloys: In $MoNb_3$, $NbTi_2Zr$, and NbTiZr, respectively, atomistic simulations or experiments found that the ratios in the CRSS between the long screw and long edge dislocations are 2, 6.3, and 2.[12,23,24] These results suggest that both edge and screw dislocations play an important role in the plasticity of BCC concentrated alloys.[25,26]

The kinks on long dislocations in both BCC pure metals and RMPEAs indicate that the dislocation lines in simulations need to be at least several times longer than the kink width for the

dislocation dynamics to be length-independent, i.e., free of any length-related artifact.[22] In what follows, we term this minimum length as the characteristic length of the dislocation, L_c. Physically, L_c is the minimum length that can represent key dynamic features of a long dislocation, and so simulations of dislocations shorter than L_c are not very meaningful. Analytical models predicted that, for screw dislocations in $Nb_xTi_{1-2x}Zr_x$ RMPEAs, $L_c = 22$–36 nm;[27] for edge dislocations, in MoNbTaVW family and NbTaV RMPEAs, respectively, $L_c = 16$–25 and 12 nm,[22,23] with the former validated by atomistic simulations. The fact that L_c is generally smaller for edge dislocations than screw ones is consistent with the former's narrower kinks. However, it remains unknown whether a dislocation's CRSS would converge to a near constant when it is longer than L_c. The main goal of this Letter is to answer this question through systematic atomistic simulations.

3D simulation cells, illustrated in Fig. 1, are constructed with three chemical elements randomly assigned to BCC lattice sites. In Fig. S1 of the supplementary material, selected atomistic structures in NbTiZr are presented and the Warren–Cowley parameters are found to be small, confirming the very low degree of chemical short-range order (CSRO) in our models. A single dislocation is built into each cell by applying the corresponding isotropic elastic displacement fields to all atoms.[28,29] Edge and screw dislocations on {110} and {112} planes are studied, except the {110} screw dislocation because it may be unstable in either BCC pure metals[18] or RMPEAs.[30,31] We remark that most prior atomistic simulations of long dislocation gliding in RMPEAs only considered slips on {110} planes, with a few exceptions that studied slips on {112}[27,32] and {123}[32] planes. On the other hand, a TEM study in MoNbTi[32] found that slips on high-order planes, such as {112}, {123}, and {134}, predominate. As will be shown later, the characteristic length of the edge dislocation is the same for {110} and {112} planes. Hence, we expect that the characteristic length would be similar for the higher-order planes, i.e., {123} and {134}.

Periodic boundary conditions are applied on the x and z directions, while the y boundaries are non-periodic. This configuration, called "periodic array of dislocations," was found to provide a better estimate of the Peierls stress in Nb than other configurations.[33] Let L_x, L_y, and L_z be the edge lengths of the cell along the three directions, respectively. For all cells, $L_x \approx 40$ nm and $L_y \approx 50$ nm, following Ref. 34. The dislocation line length $L_0 = L_z$. To study the effects of L_0, we choose seven L_z: 1, 5, 10, 20, 30, 40, and 50 nm. Accordingly, the smallest and largest cells, respectively, contain about 0.09×10^6 and 6.5×10^6 atoms.

The embedded-atom method potentials used in our recent work[30,32,37] are employed here to describe the interatomic interactions in the two alloys, two artificial pure metals, and one natural pure metal, Nb. For each dislocation on each slip plane in each alloy, five random atomic distributions of the three elements are studied and their mean and standard deviation in the critical stresses are reported. This number is sufficiently large, compared to the 3–5[38,39] and 3[12] random structures, respectively, used to study dislocation gliding in face-centered cubic (FCC) FeNi and BCC NbTiZr. We will not study the effects of the CSRO on dislocation behaviors, which were recently investigated in several BCC MPEAs.[40–43] For each pure metal, only one atomic structure is used for each dislocation. The two artificial pure metals—homogeneous MoNbTi and homogeneous NbTiZr—are simulated via A-atom potentials,[37] and the results are denoted by $MoNbTi_A$ and $NbTiZr_A$, respectively.

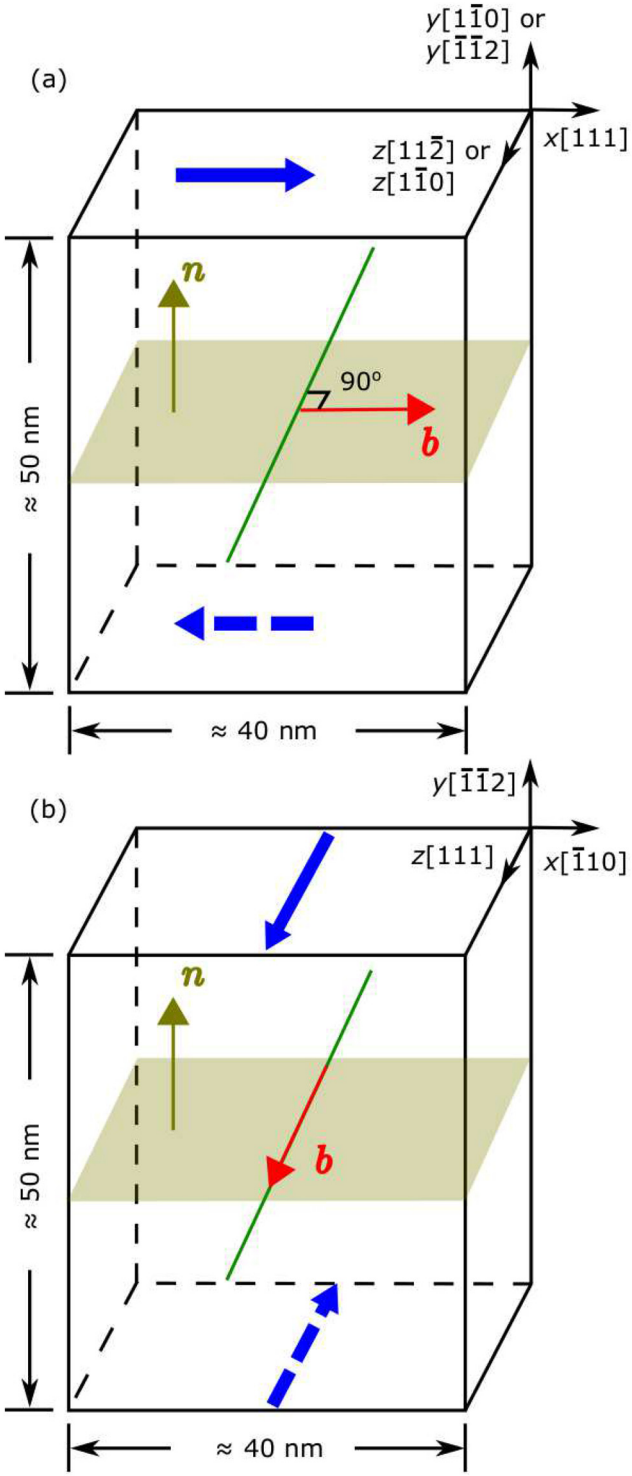

FIG. 1. Simulation box setup for (a) an edge and (b) a screw dislocation. In each subfigure, the dislocation line, Burgers vector, slip plane, and shearing directions are indicated by a green line, a red arrow, a light-brown parallelogram, and two blue arrows, respectively.

Atomistic simulations are carried out using LAMMPS.[44] First, a dynamic relaxation step was conducted for 10 ps using an NPT ensemble at 5 K and zero strain with a time step size of 1 fs. Then, a shear strain tensor $\Delta\epsilon$ with one component being non-zero is applied to each cell and with all other eight strain components set to zero. For a screw and an edge dislocation, respectively, the non-zero strain components are $\Delta\epsilon_{yz}$ and $\Delta\epsilon_{xy}$. In all cases, the strain rate is 10^7 s^{-1}. The constant applied strain rate loading mode was shown to be a better choice in critical stress calculations than the constant applied stress loading mode.[34] On the {112} plane, the dislocation, either edge or screw, moves along the twinning direction.[33] Along the y axis, the simulation cell is divided into three types of regions: two boundary regions, two buffer regions, and a central region which contains the dislocation. During the deformation, atoms within the boundary regions are continuously displaced to create shearing. An NVT ensemble is adopted in the buffer regions to keep a constant temperature of 5 K while an NVE ensemble is applied to the remaining three regions.[34] The low temperature is selected because we want to focus on the line-length-dependence without the additional influence of temperature. To account for the thermal fluctuation, three different temperature damping parameters are used for each case in Nb. Simulations stop when the non-zero strain component reaches 0.035 and 0.05, respectively, for the edge and screw dislocations, which are sufficient for the dislocation to move through the entire simulation cell at least once. Effects of some model settings are analyzed in Sec. II of the supplementary material.

Figure 2(a) presents stress–strain curves measured based on glide of dislocations ($L_0 = 50$ nm) in NbTiZr. Figures 2(b)–2(d) show that, subject to zero strain, both edge and screw dislocations possess a wavy configuration as a result of the complex energy landscapes,[45] in contrast to the straight dislocations in pure metals.[32,46] On each stress–strain curve, multiple local maxima and minima exist. In pure metals, the first local stress maximum is a result of the entire dislocation line moving.[18,33] However, in NbTiZr, the first local peak stress, i.e., points B1, C1, and D1 in Fig. 2(a), correspond to the bow-out of a short segment from its original position [gray atoms in Figs. 2(b)–2(d)]. We refer to this first local peak stress as the "initial CRSS (ICRSS)." As the strain increases, the remaining segments of the dislocation move as

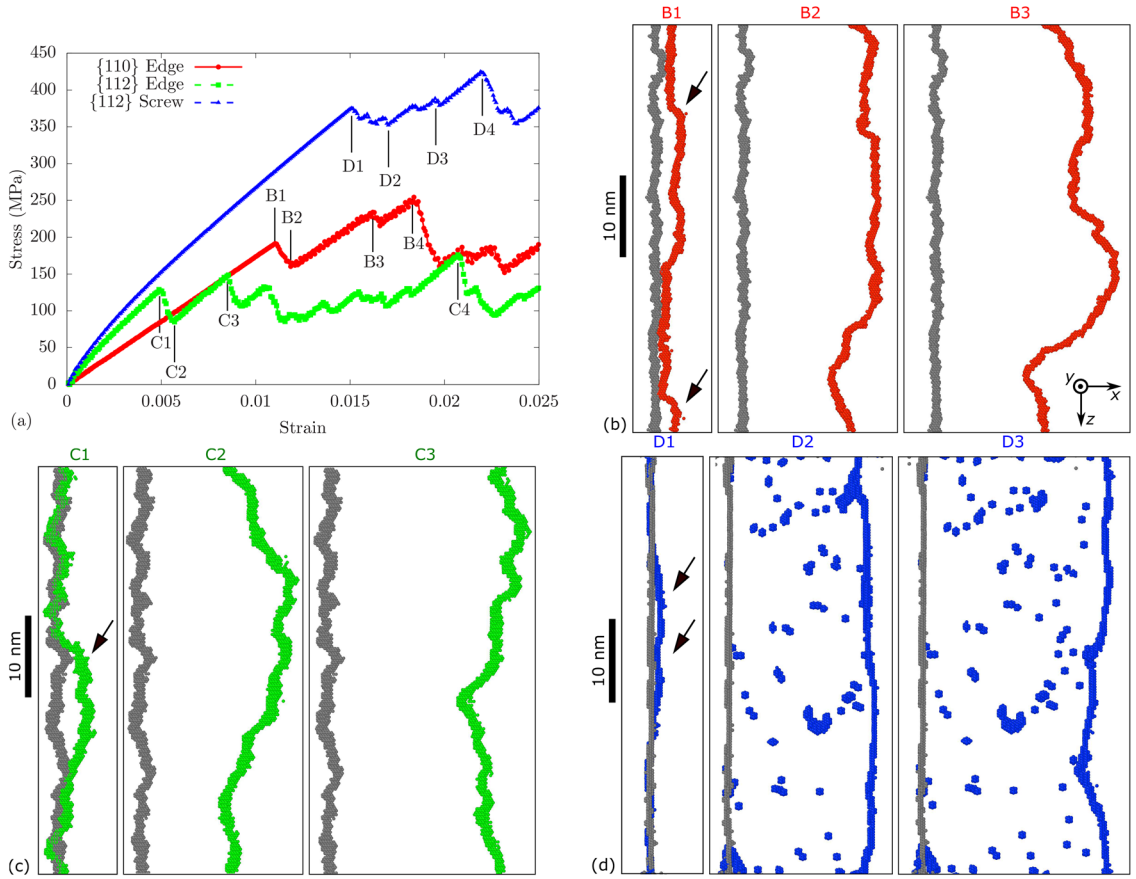

FIG. 2. (a) Stress–strain curves measured based on the deformed simulation cells that contain either an edge or a screw dislocation. (b) A {110} edge dislocation subject to zero strain (origin in (a)) is formed by gray atoms, while those corresponding to points B1, B2, and B3 in (a) consist of red atoms. Atoms at BCC lattice sites, identified by the polyhedral template matching method,[35] are deleted to aid visualization of the defects. (c) and (d) are similar to (b), except that the green and blue atoms, respectively, form an edge and a screw dislocation on the {112} plane. In (b)–(d), atomistic structures are visualized using OVITO[36] while views are illustrated by the axes in (b); the first snapshots, where some kinks are pointed to by arrows, are taken right after the first peaks (points B1, C1, and D1), before which the dislocations did not move at all. All results in this figure are based on $L_0 = 50$ nm in NbTiZr.

well. However, in most cases, the dislocation arrests after gliding over a short distance, e.g., at points B2, C2, and D2 in Fig. 2(a). Higher stresses, e.g., the stresses at points B3, C3, and D3, are then required to drive the dislocation to move further. The morphology of the gliding dislocation is wavy and constantly changing due to the local chemical composition fluctuations, as shown in Figs. S2–S4 in the supplementary material and as confirmed by our recent phase-field dislocation dynamics simulations in MoNbTi.[47,48] Eventually, at a sufficiently high stress, the dislocation glides through the entire simulation cell. This critical stress, e.g., at points B4, C4, and D4 in Fig. 2(a), is the CRSS.

While Fig. 2 is for NbTiZr only, we find that stress–strain responses (Fig. S8 in the supplementary material) and dislocation behaviors in MoNbTi are similar. Also, in both RMPEAs, when $L_0 > 5$ nm (a similar critical length was found in Fe),[49] the gliding screw dislocation leaves behind a large amount of vacancies and interstitials on the slip plane, while the gliding edge dislocation on either slip plane does not for any L_0. Since the screw dislocation does not cross slip on the {112} plane, the former phenomenon is a result of the collision of cross kinks and has been observed in prior atomistic simulations and TEM studies of gliding screw dislocation or dislocation loop expansion in $Co_{16.67}Fe_{36.67}Ni_{16.67}Ti_{30}$,[14,40,46] HfNbTiZr,[21] NbTaV,[27] and NbTiZr,[12,40] but much less pronounced in MoNbTaW.[42,46] Note that the formation of debris in the wake of a gliding screw dislocation may be unique to BCC MPEAs, since it has not been observed in FCC MPEAs.[50,51]

Values of all CRSS and ICRSS in both RMPEAs are presented in Figs. 3(a) and 3(b). We first compare some of them with those in the literature. For an edge dislocation on the {110} plane with $L_0 = 50$ nm in NbTiZr, the CRSS is 250 MPa, which agrees well with 280 MPa measured by prior atomistic simulations[12] of the same dislocation with the same length at the same temperature (5 K). On the {112} plane in MoNbTi, when $L_0 = 50$ nm, the calculated CRSS for an edge and a screw dislocation at 5 K are 498 and 1034 MPa, respectively, both of which are, as expected, higher than the CRSS measured by a room temperature TEM study, 455 MPa.[32] Generally, for the same type of dislocations, the critical stresses in MoNbTi are about twice those in NbTiZr.

Regarding the dislocation line length L_0-dependence, both CRSS and ICRSS decrease sharply when L_0 increases from 1 to 5 nm. The decrease in the critical stress is associated with the change from no kink formed (when $L_0 = 1$ nm) to a single kink-pair formed on the dislocation (when $L_0 = 5$ nm). Then, when $L_0 = 10$–20 nm, two or three narrowly spaced kink-pairs were formed, and both critical stresses decrease further. As L_0 increases further, however, both CRSS

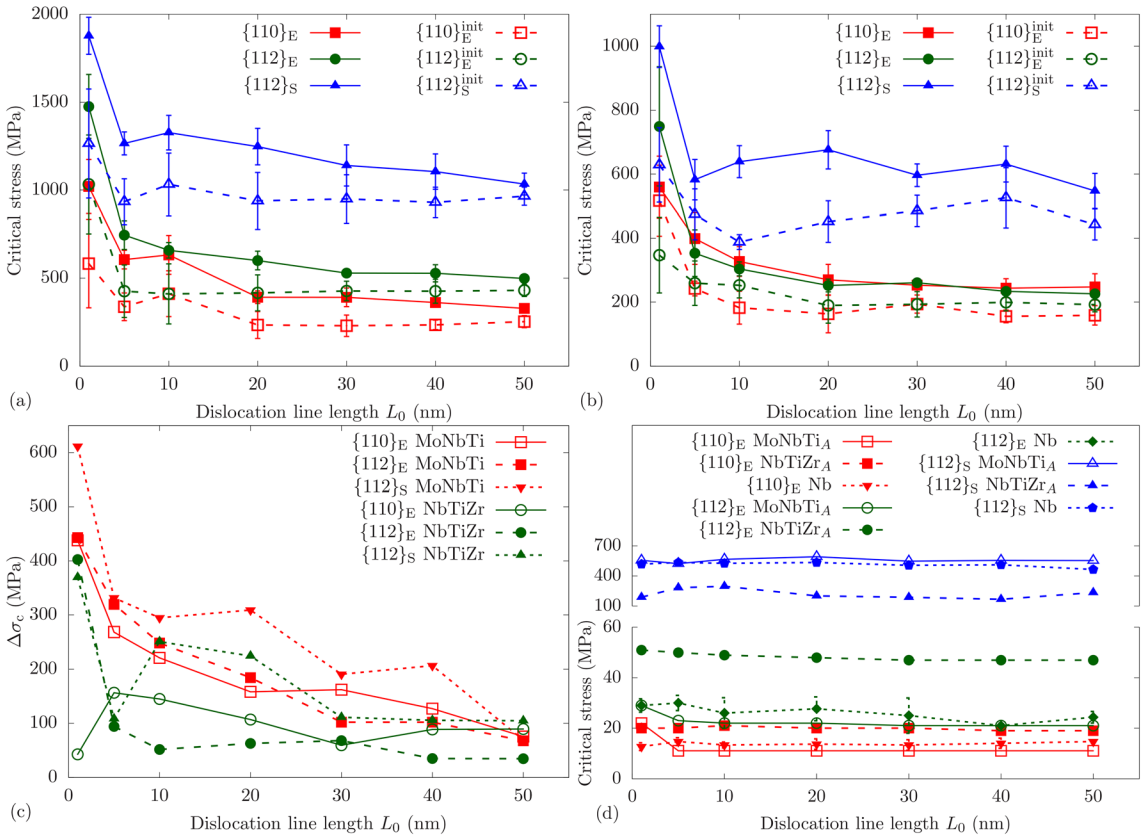

FIG. 3. Line-length-dependent CRSS and ICRSS (denoted by superscript "init") of edge (subscript "E") and screw (subscript "S") dislocations on the {110} or {112} planes in (a) MoNbTi, (b) NbTiZr, as well as (d) three pure metals: homogeneous MoNbTi, homogeneous NbTiZr, and Nb. (c) The differences between CRSS and ICRSS in the two RMPEAs. In (a) and (b), the error bars represent the standard deviations among five random atomic distributions. In (d), the error bars for Nb represent the standard deviations among results based on three temperature damping parameters used in the NVT ensemble.

TABLE I. Columns 2–5 are input parameters used in Eqs. (1) and (2) for the two RMPEAs, including the Burgers vector magnitude b (in nm), isotropic shear modulus in Hills form μ (in GPa), kink formation energy E_k (in meV), and the net dislocation/solute interaction energy over adjacent Peierls valleys $\Delta\tilde{E}_p$ (in meV). Columns 6–9 are outputs of Eqs. (1) and (2): characteristic length for kink formation, ζ_c (in nm), and characteristic length for CRSS, L_c (in nm), of edge (superscript "E") and screw (superscript "S") dislocations.

	b	μ	E_k	$\Delta\tilde{E}_p$	ζ_c^E	ζ_c^S	L_c^E	L_c^S
MoNbTi	0.28	66.38	559.87	159.5	1.37	4.05	7.67	20.66
NbTiZr	0.294	33.61	255	71	1.72	4.45	9.63	22.7

and ICRSS become length insensitive within the statistical dispersion, and the stress oscillation is reduced (Fig. S8 in the supplementary material). At these L_0, widely spaced kink-pairs were formed, as indicated by arrows in Figs. 2(b)–2(d). Taken together, our atomistic simulations determine that, in MoNbTi, the characteristic length $L_c = 25$ nm for both edge and screw dislocations and in NbTiZr, $L_c = 15$ and 25 nm, respectively, for edge and screw dislocations.

Recently, Maresca and Curtin proposed analytical models to estimate the characteristic length of the edge (superscript "E")[23] and screw (superscript "S")[27] dislocations in BCC MPEAs, i.e.,

$$L_c^E = 5.6\zeta_c^E = 5.6 \times 1.726\left[\frac{\mu^2 b^9}{144(\Delta\tilde{E}_p)^2}\right]^{\frac{1}{3}}, \quad (1)$$

$$L_c^S = 5.1\zeta_c^S = 5.1 \times 1.173\left(\frac{E_k}{\Delta\tilde{E}_p}\right)^2 b, \quad (2)$$

where ζ_c is the characteristic length for kink formation, b is the magnitude of the Burgers vector, μ is the isotropic shear modulus, E_k is the kink formation energy, and $\Delta\tilde{E}_p$ is the net dislocation/solute interaction energy over adjacent Peierls valleys. Values of the last four parameters in two RMPEAs are taken from Refs. 27 and 37 and are summarized in Table I. Values of E_k and $\Delta\tilde{E}_p$ for MoNbTi are taken from those for $Mo_{0.69}Nb_{0.31}$,[27] which has the same atomic size mismatch[52] as MoNbTi. Substituting these parameters into Eqs. (1) and (2) yields ζ_c and L_c, whose values are presented in Table I. While analytically derived L_c is for CRSS only, its values, 7.67–22.7 nm, agree well with that from present atomistic simulations for both CRSS and ICRSS, 15 or 25 nm.

The differences between CRSS and ICRSS, $\Delta\sigma_c$, are summarized in Fig. 3(c). In the same RMPEA, the screw dislocation generally possesses a higher $\Delta\sigma_c$ than the edge one. When $L_0 = 50$ nm, $\Delta\sigma_c = 68$–75 MPa in MoNbTi and 34–105 MPa in NbTiZr, suggesting that CRSS is 7%–68% higher than ICRSS.

In the three pure metals, the first local peak stresses are taken as the CRSS, which are much less dependent on L_0, as shown in Fig. 3(d), suggesting that L_c is near zero. Note that Eqs. (1) and (2) are only applicable to alloys where the dislocation/solute interactions are strong as they are in the two RMEPAs of interest, not pure metals. Once the CRSS is reached, the dislocation glides continuously. In most cases, the CRSS in Nb is lower than that in $MoNbTi_A$ but higher than that in $NbTiZr_A$. In addition, compared with their alloy counterparts, artificial pure metals have much lower CRSS due to their lack of lattice distortion. For example, for a screw dislocation on the {112} plane with $L_0 = 50$ nm, the CRSS in MoNbTi and $MoNbTi_A$ is 1034 and 554 MPa, respectively. For an edge dislocation of the same length on the same slip plane, the two CRSS are 498 and 21 MPa, respectively.

Our recent work on local slip resistances (LSR) of short dislocations ($L_0 \approx 1$ nm) found that differences in LSR among various glide planes and character angles were much lower in five RMPEAs than in their A-atom counterparts and six constituent BCC metals: Cr, Mo, Nb, Ta, V, and W.[30,31] Here, we explore whether this is also the case for the CRSS of long dislocations. To this purpose, two quantities are calculated to exhibit the slip resistance anisotropy. The first one is the ratio of the CRSS on the {112} plane to that on the {110} plane, both for the edge dislocation. The second quantity is the ratio of the CRSS of a screw dislocation to that of an edge dislocation, both on the {112} plane. Figure 4 shows that both ratios are lower in the two RMPEAs than in the three pure metals and that these ratios are largely insensitive to L_0. In particular, when $L_0 = 50$ nm, the second ratios are 2.08 and 2.42, respectively, in MoNbTi and NbTiZr. Prior atomistic simulations of long dislocation gliding calculated the screw-to-edge ratio in CRSS on {110} planes, finding it to be 2 in both $MoNb_3$[23] and NbTiZr.[12]

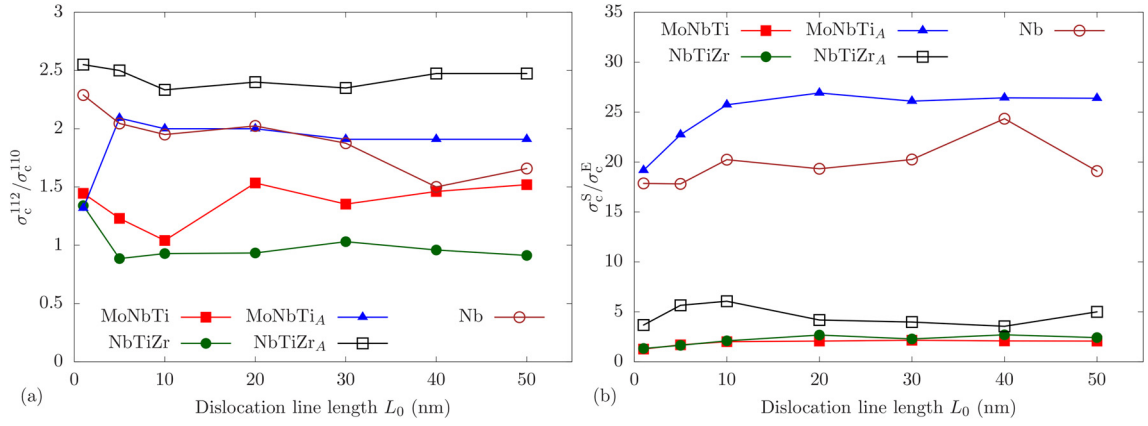

FIG. 4. (a) The {112}-to-{110} ratio in the CRSS of the edge dislocation and (b) the screw-to-edge ratio in the CRSS on the {112} plane in two RMPEAs and three pure metals.

In this Letter, we conduct atomistic simulations to calculate the CRSS and ICRSS for dislocation glide in two RMPEAs: MoNbTi and NbTiZr. Edge dislocations on both {110} and {112} slip planes, as well as screw dislocations on the {112} plane, are considered. As references, the CRSS of the same dislocations in homogeneous MoNbTi, homogeneous NbTiZr, and Nb are also calculated. In each case, seven dislocation line lengths, varying from 1 to 50 nm, are chosen. Main findings are summarized as follows:

(1) In RMPEAs, small dislocation segments bow out when the ICRSS is reached. As the strain increases further, the entire dislocation line moves, but may be later arrested, until a higher stress, i.e., CRSS, is applied to drive the dislocation to move continuously in the lattice.
(2) In RMPEAs, the gliding screw dislocation leaves behind a large number of vacancies and interstitials, as a result of the collision of cross kinks. This phenomenon does not occur in the wake of a gliding edge dislocation.
(3) In RMPEAs, the dependence of CRSS and ICRSS on length becomes undetectable within the statistical dispersion once the dislocation line is longer than 25 nm, as a result of the change in dislocation behavior.
(4) The CRSS anisotropy, quantifying the differences in CRSS among slip modes, is greatly reduced in RMPEAs than pure metals, providing direct evidence of the homogeneous plasticity in RMPEAs observed in prior TEM experiments.[32]

Despite the large differences in the critical stresses between the two RMPEAs, their stress–strain responses, CRSS anisotropy, characteristic dislocation lengths, and dislocation behaviors are similar. These findings, thus, could likely apply to other three-element RMPEAs. Future work may consider line-length-dependent dislocation mobility, which has been studied in an FCC concentrated alloy[53] but not in any RMPEAs.

See the supplementary material for information as referred to in the main text.

The authors thank Professor Fulin Wang, Professor Liming Xiong, Professor Suzhi Li, Dr. Satish Rao, and Dr. Edwin Antillon for helpful discussions. S. X. and I. J. B. gratefully acknowledge support from the Office of Naval Research under contract ONR BRC Grant N0. N00014-21-1-2536. W.-R. J. would like to acknowledge funding from the Office of Naval Research under Grant No. N000141712810. Use was made of computational facilities purchased with funds from the National Science Foundation (No. CNS-1725797) and administered by the Center for Scientific Computing (CSC). The CSC is supported by the California NanoSystems Institute and the Materials Research Science and Engineering Center (MRSEC; No. NSF DMR 1720256) at UC Santa Barbara.

AUTHOR DECLARATIONS

Conflict of Interest

The authors have no conflicts to disclose.

DATA AVAILABILITY

The data that support the findings of this study are available from the corresponding author upon reasonable request.

REFERENCES

[1]S. Naamane, G. Monnet, and B. Devincre, "Low temperature deformation in iron studied with dislocation dynamics simulations," Int. J. Plast. **26**, 84–92 (2010).
[2]L.-Q. Chen, C.-Y. Wang, and T. Yu, "Atomistic simulation of kink structure on edge dislocation in bcc iron," Chin. Phys. B **17**, 662–668 (2008).
[3]T. D. Swinburne, S. L. Dudarev, S. P. Fitzgerald, M. R. Gilbert, and A. P. Sutton, "Theory and simulation of the diffusion of kinks on dislocations in bcc metals," Phys. Rev. B **87**, 064108 (2013).
[4]G. Monnet and D. Terentyev, "Structure and mobility of the $\frac{1}{2}\langle 111\rangle\{112\}$ edge dislocation in bcc iron studied by molecular dynamics," Acta Mater. **57**, 1416–1426 (2009).
[5]S. Queyreau, J. Marian, M. R. Gilbert, and B. D. Wirth, "Edge dislocation mobilities in bcc Fe obtained by molecular dynamics," Phys. Rev. B **84**, 064106 (2011).
[6]J. Chang, V. V. Bulatov, and S. Yip, "Molecular dynamics study of edge dislocation motion in a bcc metal," J. Comput.-Aided Mater. Des. **6**, 165–173 (1999).
[7]L. Proville, L. Ventelon, and D. Rodney, "Prediction of the kink-pair formation enthalpy on screw dislocations in α-iron by a line tension model parametrized on empirical potentials and first-principles calculations," Phys. Rev. B **87**, 144106 (2013).
[8]L. Dezerald, L. Proville, L. Ventelon, F. Willaime, and D. Rodney, "First-principles prediction of kink-pair activation enthalpy on screw dislocations in bcc transition metals: V, Nb, Ta, Mo, W, and Fe," Phys. Rev. B **91**, 094105 (2015).
[9]L. Ventelon, F. Willaime, and P. Leyronnas, "Atomistic simulation of single kinks of screw dislocations in α-Fe," J. Nucl. Mater. **386–388**, 26–29 (2009).
[10]R. Ji, T. Phan, H. Chen, and L. Xiong, "Quantifying the dynamics of dislocation kinks in iron and tungsten through atomistic simulations," Int. J. Plast. **128**, 102675 (2020).
[11]A. Stukowski, D. Cereceda, T. D. Swinburne, and J. Marian, "Thermally-activated non-Schmid glide of screw dislocations in W using atomistically-informed kinetic Monte Carlo simulations," Int. J. Plast. **65**, 108–130 (2015).
[12]S. I. Rao, B. Akdim, E. Antillon, C. Woodward, T. A. Parthasarathy, and O. N. Senkov, "Modeling solution hardening in BCC refractory complex concentrated alloys: NbTiZr, $Nb_{1.5}TiZr_{0.5}$ and $Nb_{0.5}TiZr_{1.5}$," Acta Mater. **168**, 222–236 (2019).
[13]O. N. Senkov, G. B. Wilks, D. B. Miracle, C. P. Chuang, and P. K. Liaw, "Refractory high-entropy alloys," Intermetallics **18**, 1758–1765 (2010).
[14]S. I. Rao, C. Varvenne, C. Woodward, T. A. Parthasarathy, D. Miracle, O. N. Senkov, and W. A. Curtin, "Atomistic simulations of dislocations in a model BCC multicomponent concentrated solid solution alloy," Acta Mater. **125**, 311–320 (2017).
[15]S. Yin, J. Ding, M. Asta, and R. O. Ritchie, "Ab initio modeling of the energy landscape for screw dislocations in body-centered cubic high-entropy alloys," npj Comput. Mater. **6**, 110 (2020).
[16]B. Akdim, C. Woodward, S. Rao, and E. Antillon, "Predicting core structure variations and spontaneous partial kink formation for 1/2 ⟨111⟩ screw dislocations in three BCC NbTiZr alloys," Scr. Mater. **199**, 113834 (2021).
[17]C. R. Weinberger, G. J. Tucker, and S. M. Foiles, "Peierls potential of screw dislocations in bcc transition metals: Predictions from density functional theory," Phys. Rev. B **87**, 054114 (2013).
[18]X. Wang, S. Xu, W.-R. Jian, X.-G. Li, Y. Su, and I. J. Beyerlein, "Generalized stacking fault energies and Peierls stresses in refractory body-centered cubic metals from machine learning-based interatomic potentials," Comput. Mater. Sci. **192**, 110364 (2021).
[19]X. Zhou, S. He, and J. Marian, "Cross-kinks control screw dislocation strength in equiatomic bcc refractory alloys," Acta Mater. **211**, 116875 (2021).
[20]X. Zhou and J. Marian, "Temperature and stress dependence of screw dislocation nobility in Nb-V-Ta alloys using kinetic Monte Carlo simulations," Front. Mater. **8**, 801141 (2021).

[21]Y. Bu, Y. Wu, Z. Lei, X. Yuan, H. Wu, X. Feng, J. Liu, J. Ding, Y. Lu, H. Wang, Z. Lu, and W. Yang, "Local chemical fluctuation mediated ductility in body-centered-cubic high-entropy alloys," Mater. Today **46**, 28–34 (2021).
[22]R. E. Kubilay, A. Ghafarollahi, F. Maresca, and W. A. Curtin, "High energy barriers for edge dislocation motion in body-centered cubic high entropy alloys," npj Comput. Mater. **7**, 112 (2021).
[23]F. Maresca and W. A. Curtin, "Mechanistic origin of high strength in refractory BCC high entropy alloys up to 1900K," Acta Mater. **182**, 235–249 (2020).
[24]F. Mompiou, D. Tingaud, Y. Chang, B. Gault, and G. Dirras, "Conventional vs harmonic-structured β-Ti-25Nb-25Zr alloys: A comparative study of deformation mechanisms," Acta Mater. **161**, 420–430 (2018).
[25]C. Lee, G. Kim, Y. Chou, B. L. Musicó, M. C. Gao, K. An, G. Song, Y.-C. Chou, V. Keppens, W. Chen, and P. K. Liaw, "Temperature dependence of elastic and plastic deformation behavior of a refractory high-entropy alloy," Sci. Adv. **6**, eaaz4748 (2020).
[26]C. Lee, F. Maresca, R. Feng, Y. Chou, T. Ungar, M. Widom, K. An, J. D. Poplawsky, Y.-C. Chou, P. K. Liaw, and W. A. Curtin, "Strength can be controlled by edge dislocations in refractory high-entropy alloys," Nat. Commun. **12**, 5474 (2021).
[27]F. Maresca and W. A. Curtin, "Theory of screw dislocation strengthening in random BCC alloys from dilute to "High-Entropy" alloys," Acta Mater. **182**, 144–162 (2020).
[28]S. Xu, L. Smith, J. R. Mianroodi, A. Hunter, B. Svendsen, and I. J. Beyerlein, "A comparison of different continuum approaches in modeling mixed-type dislocations in Al," Modell. Simul. Mater. Sci. Eng. **27**, 074004 (2019).
[29]S. Xu, Y. Su, and I. J. Beyerlein, "Modeling dislocations with arbitrary character angle in face-centered cubic transition metals using the phase-field dislocation dynamics method with full anisotropic elasticity," Mech. Mater. **139**, 103200 (2019).
[30]S. Xu, Y. Su, W.-R. Jian, and I. J. Beyerlein, "Local slip resistances in equal-molar MoNbTi multi-principal element alloy," Acta Mater. **202**, 68–79 (2021).
[31]R. A. Romero, S. Xu, W.-R. Jian, I. J. Beyerlein, and C. Ramana, "Atomistic simulations of the local slip resistances in four refractory multi-principal element alloys," Int. J. Plast. **149**, 103157 (2022).
[32]F. Wang, G. H. Balbus, S. Xu, Y. Su, J. Shin, P. F. Rottmann, K. E. Knipling, J.-C. Stinville, L. H. Mills, O. N. Senkov, I. J. Beyerlein, T. M. Pollock, and D. S. Gianola, "Multiplicity of dislocation pathways in a refractory multiprincipal element alloy," Science **370**, 95–101 (2020).
[33]W.-R. Jian, S. Xu, and I. J. Beyerlein, "On the significance of model design in atomistic calculations of the Peierls stress in Nb," Comput. Mater. Sci. **188**, 110150 (2021).
[34]W.-R. Jian, M. Zhang, S. Xu, and I. J. Beyerlein, "Atomistic simulations of dynamics of an edge dislocation and its interaction with a void in copper: A comparative study," Modell. Simul. Mater. Sci. Eng. **28**, 045004 (2020).
[35]P. M. Larsen, S. Schmidt, and J. Schiøtz, "Robust structural identification via polyhedral template matching," Modell. Simul. Mater. Sci. Eng. **24**, 055007 (2016).
[36]A. Stukowski, "Visualization and analysis of atomistic simulation data with OVITO—The Open Visualization Tool," Modell. Simul. Mater. Sci. Eng. **18**, 015012 (2010).
[37]S. Xu, E. Hwang, W.-R. Jian, Y. Su, and I. J. Beyerlein, "Atomistic calculations of the generalized stacking fault energies in two refractory multi-principal element alloys," Intermetallics **124**, 106844 (2020).
[38]Y. N. Osetsky, G. M. Pharr, and J. R. Morris, "Two modes of screw dislocation glide in FCC single-phase concentrated alloys," Acta Mater. **164**, 741–748 (2019).
[39]V. Turlo and T. J. Rupert, "Interdependent linear complexion structure and dislocation mechanics in Fe-Ni," Crystals **10**, 1128 (2020).
[40]E. Antillon, C. Woodward, S. I. Rao, and B. Akdim, "Chemical short range order strengthening in BCC complex concentrated alloys," Acta Mater. **215**, 117012 (2021).
[41]L. Zhao, H. Zong, X. Ding, and T. Lookman, "Anomalous dislocation core structure in shock compressed bcc high-entropy alloys," Acta Mater. **209**, 116801 (2021).
[42]S. Yin, Y. Zuo, A. Abu-Odeh, H. Zheng, X.-G. Li, J. Ding, S. P. Ong, M. Asta, and R. O. Ritchie, "Atomistic simulations of dislocation mobility in refractory high-entropy alloys and the effect of chemical short-range order," Nat. Commun. **12**, 4873 (2021).
[43]S. Mishra, S. Maiti, and B. Rai, "Computational property predictions of Ta-Nb-Hf-Zr high-entropy alloys," Sci. Rep. **11**, 4815 (2021).
[44]S. Plimpton, "Fast parallel algorithms for short-range molecular dynamics," J. Comput. Phys. **117**, 1–19 (1995).
[45]E. Antillon, C. Woodward, S. I. Rao, B. Akdim, and T. A. Parthasarathy, "A molecular dynamics technique for determining energy landscapes as a dislocation percolates through a field of solutes," Acta Mater. **166**, 658–676 (2019).
[46]B. Chen, S. Li, H. Zong, X. Ding, J. Sun, and E. Ma, "Unusual activated processes controlling dislocation motion in body-centered-cubic high-entropy alloys," Proc. Natl. Acad. Sci. U. S. A. **117**, 16199–16206 (2020).
[47]L. T. W. Smith, Y. Su, S. Xu, A. Hunter, and I. J. Beyerlein, "The effect of local chemical ordering on Frank-Read source activation in a refractory multi-principal element alloy," Int. J. Plast. **134**, 102850 (2020).
[48]L. T. W. Fey, S. Xu, Y. Su, A. Hunter, and I. J. Beyerlein, "Transitions in the morphology and critical stresses of gliding dislocations in multiprincipal element alloys," Phys. Rev. Mater. **6**, 013605 (2022).
[49]J. Marian, W. Cai, and V. V. Bulatov, "Dynamic transitions from smooth to rough to twinning in dislocation motion," Nat. Mater. **3**, 158–163 (2004).
[50]S. I. Rao, C. Woodward, T. A. Parthasarathy, and O. Senkov, "Atomistic simulations of dislocation behavior in a model FCC multicomponent concentrated solid solution alloy," Acta Mater. **134**, 188–194 (2017).
[51]E. Antillon, C. Woodward, S. I. Rao, B. Akdim, and T. A. Parthasarathy, "Chemical short range order strengthening in a model FCC high entropy alloy," Acta Mater. **190**, 29–42 (2020).
[52]S. Xu, S. Z. Chavoshi, and Y. Su, "On calculations of basic structural parameters in multi-principal element alloys using small atomistic models," Comput. Mater. Sci. **202**, 110942 (2022).
[53]R. B. Sills, M. E. Foster, and X. W. Zhou, "Line-length-dependent dislocation mobilities in an FCC stainless steel alloy," Int. J. Plast. **135**, 102791 (2020).